Eur. Phys. J. D **8**, 451–457 (2000)

THE EUROPEAN PHYSICAL JOURNAL D

EDP Sciences

Dynamical study and control of drift waves in a magnetized laboratory plasma

E. Gravier[1], X. Caron[1], G. Bonhomme[1,a], T. Pierre[2], and J.L. Briançon[1]

[1] Laboratoire PMIA[b], Université Henri Poincaré, Nancy-I, B.P. 239, 54506 Vandœuvre-lès-Nancy Cedex, France
[2] Turbulence Plasma[c], Université de Provence, 13397 Marseille Cedex 20, France

Received 31 March 1999 and Received in final form 5 August 1999

Abstract. The various dynamical regimes of collisional drift waves in a magnetized plasma column are experimentally studied. These unstable low-frequency electrostatic waves are related with strong modulations of the ion and electron density. The angular velocity of the rotating plasma column is the control parameter of the dynamics: regular, chaotic and turbulent regimes are obtained. The spatial extension of the system allows for the occurrence of spatiotemporal chaos. The time-delay auto-synchronization method of controlling chaos [K. Pyragas, Phys. Lett. A **170**, 421 (1992)] though purely temporal is successfully applied. A numerical study using coupled nonlinear oscillators exhibiting chaos is compared to the experimental results. The control method is tested on this model.

PACS. 52.35.Kt Drift waves – 52.35.Ra Plasma turbulence – 05.45.-a Nonlinear dynamics and nonlinear dynamical systems

1 Introduction

During the last years, many works have shown the universality of different scenarios towards chaotic dynamics. In plasma physics, very few experimental works exhibiting a clear bifurcation scenario have been published. Our study is devoted to this topics in the case of unstable waves in a magnetized plasma column. The chaos control algorithms introduced recently have been successfully applied in the case of compact systems exhibiting temporal low-dimensional chaos. On the other hand, the experimental control of spatiotemporal chaos is up to now an unsolved problem. Both spatial and temporal dynamics have to be considered. For instance, only very preliminary results have been obtained in optics in the case of coupled laser diode arrays [1]. Laboratory plasmas are indeed well suited for the study owing to the existence of strong nonlinearities. The parameters can be easily chosen in order to select the dynamical regime. Most recent studies have been devoted to frequency fluctuations lower than the characteristic frequencies (*i.e.* plasma oscillations and cyclotron frequencies). Moreover, these fluctuations are frequently invoked as responsible for the anomalous radial transport of energy in tokamak plasmas leading to a lower efficiency of the reactors. More precisely, the turbulent regime of the drift waves corresponding to turbulent density fluctuations is enhancing the diffusion of the energy across the magnetic field lines. The possibility of controlling these dynamical regimes is therefore very appealing especially using a very low-level action on the system as it is the case in typical chaos control experiments.

Drift waves are naturally excited in magnetized plasmas exhibiting a radial density gradient [2,3]. Various destabilizing mechanisms have been identified. The electron collision rate or the existence of an axial electron beam have been extensively studied. This work is performed on a magnetized triple-plasma device "Mirabelle" which exhibits easily nonlinear drift waves. The characteristics of the unstable waves are indeed very different of the drift waves observed in the plasmas of the tokamaks. Indeed, very high mode numbers are excited in tokamaks drift wave turbulence and thus the plasma slab approximation is valid. On the other hand, the unstable wavelengths in our device are of the order of the plasma radius and global modes are excited. However, the dynamics is of great interest because the system is extended in space, leading to spatiotemporal characteristics. The study of the chaos control algorithms in non purely temporal systems is indeed our main goal in this study.

Two major control methods have proven their efficiency in the case of temporal chaos. The goal of the OGY method [4] is to stabilize the unstable periodic orbits (UPO) embedded in the chaotic strange attractor. Only tiny proper impulses are periodically applied to the control parameter in order to progressively set the dynamical system very close the targeted UPO. The real-time analysis of the Poincaré section is needed and practical

[a] e-mail: gerard.bonhomme@lpmi.uhp-nancy.fr
[b] ESA 7040 du CNRS
[c] UMR 6633 du CNRS

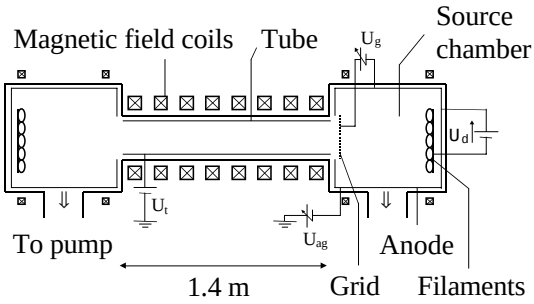

Fig. 1. The triple plasma device MIRABELLE.

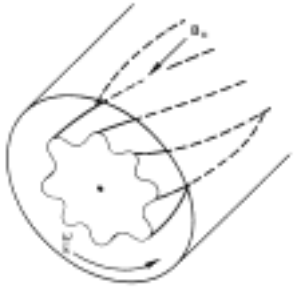

Fig. 2. Drift wave geometry [13].

implementation is often difficult. Moreover, this method is not very robust against noise because the dynamical system is indeed free to evolve between the application of the controlling pulses.

The time-delay auto-synchronization method (TDAS) proposed by Pyragas [5] allows for an easy experimental implementation. A continuous control signal is applied to the system, *i.e.* to the dynamical variable. It is elaborated from the difference between the real-time signal and the time-delayed version of this signal. The delay is chosen equal to the period of the targeted UPO. This method has already been successful applied in our group [6]. We report here on the stabilization of spatiotemporal chaos using the TDAS method.

It is worth noting that several numerical studies dealing with the control of spatiotemporal chaos have recently been performed [7–9]. However, it is hardly possible to transpose these results to a real experiment. On the other hand, other methods derived from the TDAS method have been proposed [10,11] leading to a better efficiency, *i.e.* a lower level of the control signal.

Our results are compared to the numerical results from an array of coupled oscillators. Each of them is modelling a definite region of the plasma. The comparison leads to a better understanding of the validity and the limitations of the TDAS method.

2 Experimental set-up

The experiments are performed in Mirabelle, a triple-plasma device [12] with a central plasma column immersed in a solenoid (see Fig. 1). The magnetic field is parallel to the axis of the cylinder with a typically intensity $B = 40$ mT. The plasma is created by a thermionic discharge in argon (pressure 3×10^{-4} mbar) inside one end-chamber and the ionizing electrons enter the central section following the magnetic field lines. The radial density profile is partly determined by the radial distribution of the flux of the ionizing electrons. The detailed balance between the diffusion across the field lines and the local volume recombination leads to a radial density gradient length of the order of 4 cm.

The electron temperature is 2 eV and the electron density at the center is close to 2×10^{15} m^{-3}. The density gradient is recorded using a plane Langmuir probe radially movable. The drift waves are unstable from the separation grid and they are studied in a section of the plasma column located 40 cm from the grid. The fluctuations associated to the drift waves are measured on the electron saturation current of the probe. The typical frequency range is 5 to 15 kHz. The radial position of the maximum of the amplitude coincides with the location of the maximum of the density gradient. In order to minimize the influence of the magnetic field, the measurement of the density fluctuations have to be made using the ion saturation current of the Langmuir probe because the ion Larmor radius is much larger than the size of the sheath around the probe. However, the collected current is very low, leading to a very poor signal/noise ratio. We have checked that the measurement of the relative fluctuations can be made using the electron saturation current of the cylindrical Langmuir probe. The obtained power spectra are identical though the collection of the probe is not isotropic.

The drift waves propagate azimuthally [13] (as seen in Fig. 2) and the mode number m is determined by the number of wavelength around the column. A specific set-up has been developed for the diagnostic of the mode structure [14]. An azimuthal array of 32 cylindrical Langmuir probes (0.5 mm in diameter, 4 mm in length) has been built. The tips of the probes are located on a circle with radius 7 cm. All the probes are biased beyond the plasma potential. This set-up is connected to two VXI plug-in units for the synchronous acquisition of the time-series. The sampling rate is 200 kHz (16 bits resolution) and 16 kwords are recorded. This fast acquisition system allows a real-time imaging of the spatiotemporal regime of the system.

The growth rate of the drift waves is related to the angular velocity of the plasma column [2,3]. The rotation is induced by the $\mathbf{E} \times \mathbf{B}$ drift due to the existence of a radial electric field across the plasma. This radial field can be modified by biasing an outer cylindrical tube placed inside the vacuum tube. The radial profiles of the density and potential have been recorded. The results are consistent with a parabolic profile of the potential leading to a rigid body rotation of the plasma column with no shear layer. More refined measurements using gridded probes and test waves are under achievement. The transition from a regular regime to a chaotic and turbulent regime can be studied by changing the polarisation of the tube. The next section is devoted to the detailed study of this scenario.

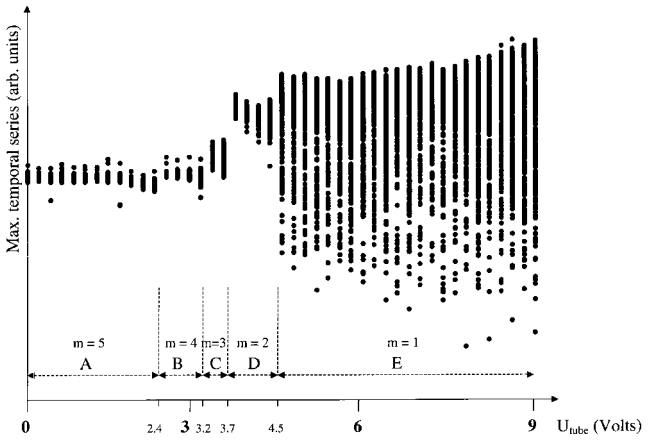

Fig. 3. First scenario (5 modes).

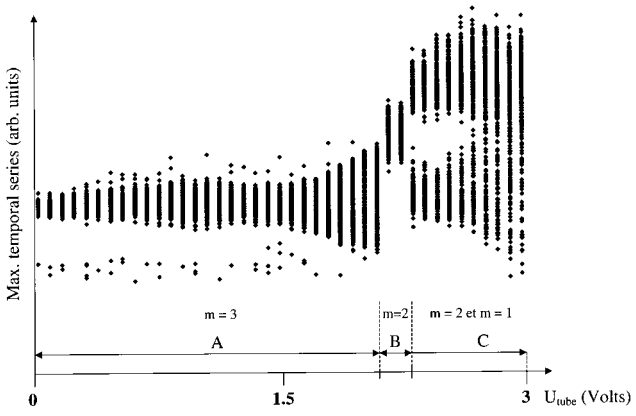

Fig. 4. Second scenario (3 modes).

3 Dynamical regimes of the drift waves

The accessible control parameter is the biasing (U_t) of the inner tube (see Fig. 1). The polarisation at the outer edge of the plasma column determines the radial electric field as consequently the $\mathbf{E} \times \mathbf{B}$ drift of the plasma column. The rigid body rotation of the column induces a Doppler shift of the unstable frequencies. The evolution of the dynamical regime is directly related to this Doppler shift. Different situations are depicted here as the polarisation of the tube is varied. The analysis is based on the sampling of the maxima inside the time-series: in a diagram depicting these maxima versus the biasing of the tube, a regular regime corresponds to a stationary value of the maxima and a unique point on the figure. On the other hand, a chaotic or a turbulent regime induces a scattering of the values of the sampled relative maxima. This bifurcation diagram allows to determine the values of the control parameter leading to a chaotic regime. This analysis is performed only in the time domain and the obtained diagram is referred to as the temporal bifurcation diagram.

As usual in experimental studies on complex dynamical systems, different bifurcation scenarios can be obtained due to the high sensitivity to the large number of influent parameters. The typical observation is that the mode number m of the unstable drift waves decreases when the plasma potential inside the source chamber is decreased by lowering the heating of the emitting filaments. This variation is correlated with the decrease of the mode number when the potential of the tube at the outer of the plasma column is increased.

Very similar bifurcation scenarios have been recently reported [15,16] on the KIWI experiment. However, only three different modes have been observed compared to five on our device. This is maybe related to a lower plasma diameter (3 cm) in the KIWI device. Indeed, we have noted on our device that the azimuthal mode number is lower when a lower plasma diameter is obtained with changing the compensation magnetic field.

Two different scenarios are reported here (see Figs. 3 and 4). The first one is obtained when the plasma potential inside the source chamber is high. In both cases, the azimuthal mode number m decreases with increasing the biasing of the outer tube, *i.e.* lowering the radial electric field. The first case is depicted in Figure 3. The control parameter is the polarisation of the tube varying from 0 to 9 volts. Starting from $m = 5$, a decrease in the mode number is recorded with increasing the voltage on the tube. The fluctuation level is continuously increasing during this variation. The labels A, B, C, D and E indicate the dominant modes corresponding to the maximum growth rate. Other modes can coexist at a lower level. When the tube voltage is $U_t = 4.5$ volts, the obtained regime is clearly chaotic. We have performed a numerical analysis of the corresponding time-series [17,18] indicating the existence of a positive Lyapunov exponent. The correlation dimension, in agreement with the Lyapunov dimension, is in the range 4.2–4.3.

The second case is depicted in Figure 4. The polarisation of the tube is varied between 0 and 3 volts. The transition scenario starting from the mode $m = 3$ is different: a quasiperiodic regime is obtained before the transition $m = 3$ to $m = 2$. The nonlinear coupling between the components of frequencies $f_1 = 5$ kHz and $f_2 = 7$ kHz leads to several peaks in the power spectrum. This situation corresponds to a mode-locking regime with two commensurable frequencies. Increasing the control parameter, a broadening of the peaks is recorded in the power spectrum ($f_1 = 5$ kHz and $f_2 = 10$ kHz). The corresponding chaotic regimes in this situation exhibit a correlation dimension again close to 4.2. The main difference between the two cases is that the different regimes are more clearly distinguished in the second case. As will be seen in the next section, we have noted that the control of the chaotic regimes is much more successful in the situation depicted in Figure 4.

4 Experimental control of the chaotic regime of drift waves

According to the TDAS method, the control signal is obtained following the control law: $[C(t) = K[S(t) - S(t - \tau)]$ [5] (see Fig. 5), where τ is the delay chosen close to the period of the targeted UPO, K is an adjustable gain and

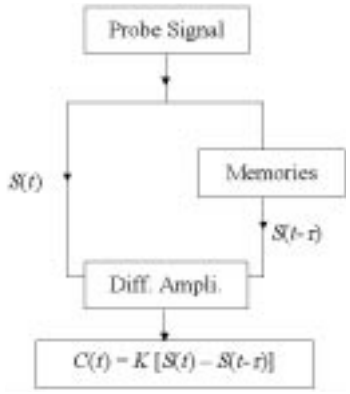

Fig. 5. The control signal is obtained by the law: $C(t) = K[S(t) - S(t-\tau)]$ [5]. The signal from the Langmuir probe is digitized and stored in FIFO memories with numerically addressed transit time. The signal is then converted back into an analog signal. The difference signal is obtained through a conventional differential amplifier.

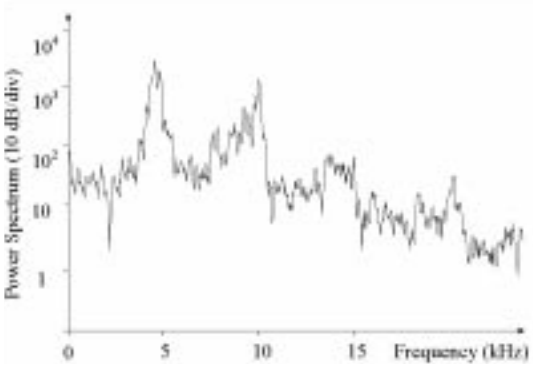

Fig. 6. Power spectrum before control.

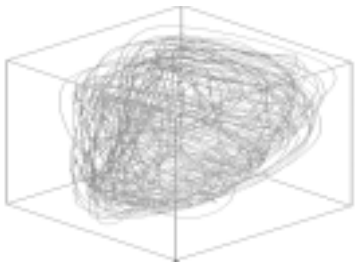

Fig. 7. Phase space attractor before control [19].

$S(t)$ is the signal originating from one selected probe of the azimuthal array. After analog to digital conversion of the real-time time series, the time-delay is produced by selecting the propagation time inside memories. The analog signal is after that reconstructed by a digital to analog converter. This control method is purely temporal since the information signal is obtained at one definite location and the control signal is applied to the control parameter. The spatiotemporal character of the dynamical regime is not taken into account.

In order to test the efficiency of the method, a slightly chaotic regime is selected (see Figs. 6 and 7). The correlation dimension in this typical case is, as previously mentioned, 4.2. The frequency spectrum exhibits two broad peaks at 5 kHz and 10 kHz. The probe is located at the maximum radial density gradient. In fact, the power spectra are almost unchanged with changing the radial position of the probe. The time-delay to be chosen in order to target the first peak is $\tau = 200\ \mu$s. The delay $\tau = 100\ \mu$s has to be chosen in the second case. The gain of the following amplifier can be selected over three decades and the control signal is applied to the tube at the outer edge of the plasma column.

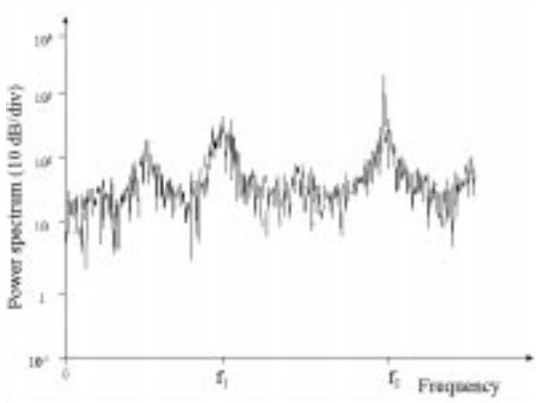

Fig. 8. Power spectrum after control. A 200 μs time delay is chosen, corresponding to the first peak (5 kHz) in the power spectrum before control.

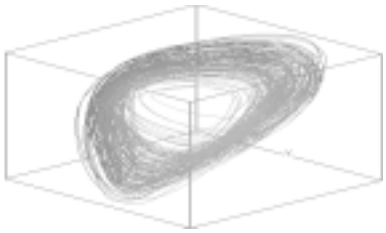

Fig. 9. Phase space attractor [19] after control. A 200 μs time delay is chosen.

The results corresponding to a delay $\tau = 200\ \mu$s are depicted in Figures 8 and 9. The gain is properly adjusted using a trial/error method in order to obtain the maximum efficiency. The modifications in the power spectrum are clearly seen. A narrowing of the peaks is obtained, mostly of the 10 kHz frequency. It is important to note that the mean value of the control signal is zero. The dynamical regime is not changed by changing the mean value of the control parameter but indeed by the dynamical action produced by the elaborated control signal. The main conclusion in this case is that, though the targeted UPO corresponds to the frequency f_1 (5 kHz), the harmonics f_2 is clearly enhanced. The spatial mode $m = 2$ is selected. In the phase space, the reconstructed attractor [19] is a limit cycle of period one related to the obtained periodic regime. There is a clear decrease of the dimensionality, but because of the noise level no reliable correlation dimension can be given. After the control is activated, the control signal decreases to a low level (below one volt) compared

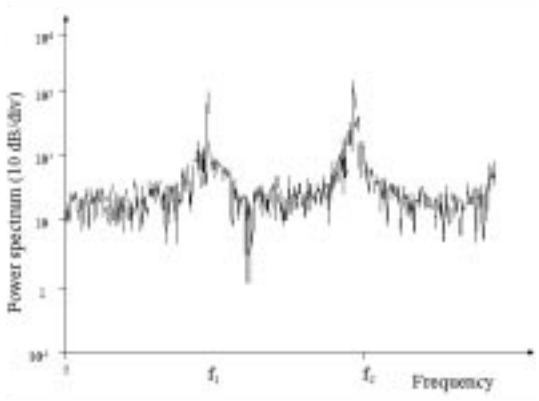

Fig. 10. Power spectrum after control. A 100 μs time delay is chosen, corresponding to the second peak (10 kHz) in the power spectrum before control.

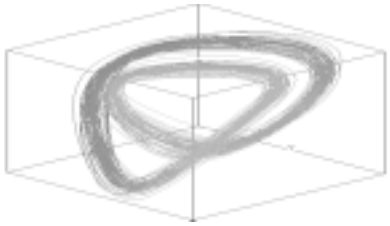

Fig. 11. Phase space attractor [19] after control. A 100 μs time delay is chosen.

to the values necessary for the whole transition scenario [16]. This is typical for a control of chaos experiment.

In the second case, the results are depicted in Figures 10 and 11 [20]. The modifications after the control are clearly seen. The power spectrum shows that the narrowing of the peaks after control. In the phase space, the attractor is an orbit corresponding to a mode-locking regime with two commensurable frequencies. In this situation, the efficiency of the TDAS method is clearly understood [21]. Moreover, using the control law $C(t)$ mentioned above, a component of period 200 μs is remaining inside the control signal obtained using a time-delay 100 μs. This low-frequency component is driving the dynamical system at the frequency 5 kHz. In fact, in the case of perfect experimental signals, the control signal would be made of two components: the first one is controlling the main frequency at 10 kHz and whose amplitude would be reduced to a very low level after the transient controlling process, and the second permanent component drives the system at 5 kHz.

Finally, we observe that the efficiency of the control method is dramatically reduced when the correlation dimension is increased, *i.e.* when the control parameter is set at a higher value. The dynamical system can no longer be described using a low number of degrees of freedom. The spatiotemporal character is then certainly much more important leading to a rapid increase of the complexity. A refined control method taking into account the spatial dynamical analysis would be required.

5 Comparison with a lattice of coupled maps

Coupled oscillators have frequently been used for modelling dynamical systems. Considering complex systems, this approach is often the easiest way to obtain useful numerical results. In particular, this strategy has been often used in the case of spatiotemporal chaos [22–35].

The system under consideration is built with a closed loop of N nonlinear oscillators. Each one is coupled to the two neighbours. The strength of the coupling is a basic modelling of the control parameter of the extended dynamical system. One could think that each oscillator is modelling a definite azimuthal region of the unstable layer.

The oscillating nonlinear function has been selected from [34] with $r = 1.65$ corresponding to a chaotic regime for each isolated oscillator. The coupling between the neighbouring oscillators is expressed as:

$$x_j^{n+1} = (1 - 2\gamma) f(x_j^n) + \gamma [f(x_{j-1}^n) + f(x_{j+1}^n)]$$

where the index n corresponds to the time step and j is used for the identification of the oscillators.

We are using here a first return map, *i.e.* the position of the dynamical variable x^{n+1} at the time $(n+1)\delta t$ is determined by the position x^n at time $n\delta t$. The study of the nonlinear flow is reduced here to the study of the dynamics along one direction corresponding to main dynamical evolution of the system. The limiting conditions are periodic and the initial values are random numbers between 0 and 1.

For a fixed γ parameter, the display of the whole set of points is informing on the dynamical regime of the system. Points located preferentially at particular positions is characteristic of a periodic regime. On the contrary, a chaotic regime is related to scattered points. The temporal evolution of the 16 oscillators in the case $\gamma = 0.29$ exhibits a chaotic regime. The analysis of the time-series from one of the oscillators shows two broad peaks in the power spectrum corresponding to two incommensurable frequencies. The implementation of the TDAS method in the same way as in the experiment described above gives numerical results in accordance with the experimental results. Indeed, even though in the numerical system no frequency selection is evident, the behaviour of the system is comparable when the control is active. No frequency selection is obtained when the chosen delay corresponds to the frequency f_1. When the delay corresponds to the frequency f_2, the frequency f_1 is reinforced in the power spectrum.

The system with various coupling is now considered: the coupling strength γ is varied from 0.225 to 0.32. Two different bifurcation diagrams are obtained. In the first one (letter a), the temporal evolution of one selected oscillator is depicted *versus* the coupling strength. In the second diagram, the spatial dynamical regime is depicted at a fixed time (letter b). Let us note again that a temporal or spatial decoherency is related to scattered points.

Figures 12 and 13 depict the system without control. With a very weak coupling strength, the time-series are similar to turbulent signals and no spatial coherency

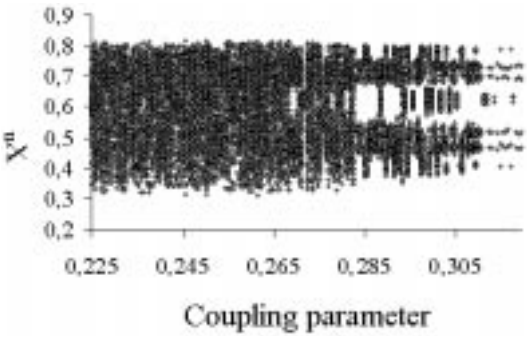

Fig. 12. Temporal bifurcation diagram (no control applied).

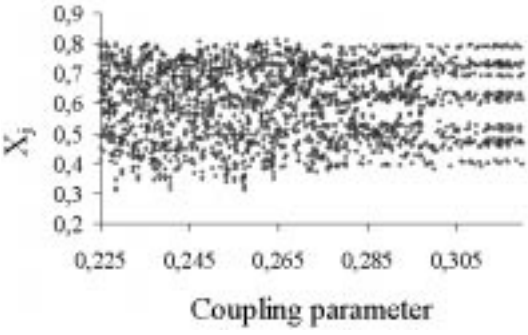

Fig. 13. Spatial bifurcation diagram (no control applied).

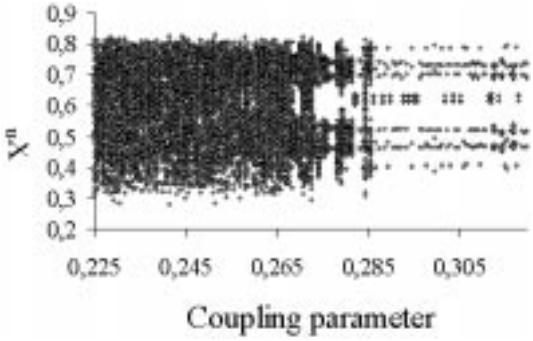

Fig. 14. Temporal bifurcation diagram (TDAS control applied).

is present. On the other hand, there is still a high correlation between spatial and temporal signals compatible with a spatiotemporal chaotic regime.

Figures 14 and 15 depict the same system with application of a generalized TDAS method. The control signal is built in the same way as in the experiment. It is elaborated from the temporal signal from one selected oscillator and the control signal (difference between the real-time and delayed signal) is applied to the whole system.

Each oscillator is controlled using his own temporal signal. Compared to the previous case, the coherence is maintained with lower values of the parameter γ. The periodicity window is enlarged and the chaotic regimes are fewer. It should be noted that the classical TDAS method allows here for an enhancement of the spatial coherency of the system. This purely temporal method is indeed of some efficiency in the case of a spatiotemporal system.

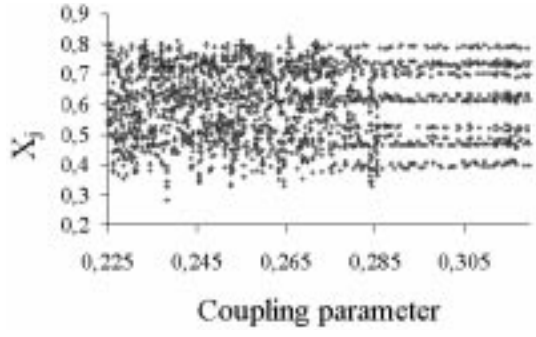

Fig. 15. Spatial bifurcation diagram (TDAS control applied).

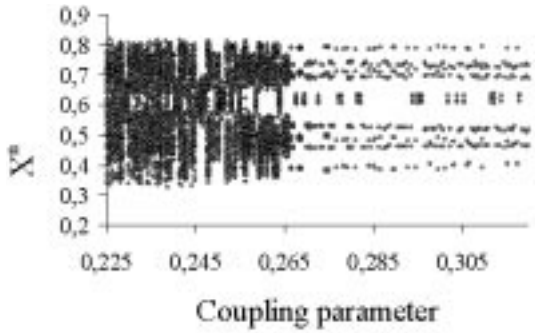

Fig. 16. Temporal bifurcation diagram (Localized TDAS control applied).

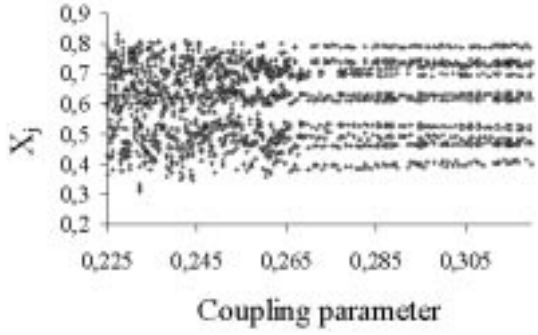

Fig. 17. Spatial bifurcation diagram (Localized TDAS control applied).

Figures 16 and 17 depict the same system with application of a localized TDAS method. Each oscillator is controlled using his own temporal signal. Compared to the previous case, the coherence is maintained with lower values of the parameter γ.

This localized TDAS method is much more efficient than the generalized TDAS method but it is certainly difficult to implement on real experiments because a spatially extended control is needed inside the plasma. In the case of the generalized TDAS method, this drawback is not present because a global external action allows for the stabilization of the chaotic regime. In conclusion, the experimental effort needed in the case of the localized TDAS method would not be relevant in the case of the drift waves.

6 Conclusion

The efficiency of the time-delay auto-synchronization method has been tested experimentally on drift waves in a magnetized laboratory plasma exhibiting spatiotemporal chaos and numerically on an array of coupled nonlinear oscillators. The method has been proved successful in the case of low-dimensional chaos. If the complexity of the dynamical regime is increased, this purely temporal method is no longer efficient and a true spatial and temporal control would be required.

We are very indebted to J.F. Pautex, C. Thiébaut for technical assistance and M. Dubuit for support in numerical analysis.

References

1. M. Munkel, F. Kaiser, O. Hess, Phys. Rev. E **56**, 3868 (1997).
2. E.M. Marshall, R.F. Ellis, J.E. Walsh, Plasma Phys. Control. Fusion **28**, 1461 (1986).
3. R.F. Ellis, E. Marden-Marshall, R. Majeski, Plasma Phys. **22**, 113 (1980).
4. E. Ott, C. Grebogy, J.A. Yorke, Phys. Rev. Lett. **64**, 1196 (1990).
5. K. Pyragas, Phys. Lett. A **170**, 421 (1992).
6. Th. Pierre, G. Bonhomme, A. Atipo, Phys. Rev. Lett. **76**, 2290 (1996).
7. M.E. Bleich, J.E.S. Socolar, Phys. Rev. E **54**, R17 (1996).
8. R.O. Grigoriev, M.C. Cross, H.G. Schuster, Phys. Rev. Lett. **79**, 2795 (1996).
9. K. He, G. Hu, Phys. Rev. E **53**, 2271 (1996).
10. S. Boccaletti, D. Maza, H. Mancini, R. Genesio, F.T. Arecchi, Phys. Rev. Lett. **79**, 5246 (1997).
11. H.G. Schuster, M.B. Stemmler, Phys. Rev. E **56**, 6410 (1997).
12. Th. Pierre, G. Leclert, F. Braun, Rev. Sci. Instrum. **58**, 6 (1987).
13. F.F. Chen, *Introduction to plasma physics and controlled fusion* (Plenum Press, New-York, 1984).
14. A. Latten, T. Klinger, A. Piel, T. Pierre, Rev. Sci. Instrum. **66**, 3254 (1995).
15. T. Klinger, A. Latten, A. Piel, G. Bonhomme, Th. Pierre, Plasma Phys. Control. Fusion **39**, B145 (1997).
16. T. Klinger, A. Latten, A. Piel, G. Bonhomme, Th. Pierre, T. Dudok de Wit, Phys. Rev. Lett. **79**, 3913 (1997).
17. H.D.I. Abarbanel, *Analysis of observed chaotic data* (Springer, 1996).
18. T.M. Kruel, M. Eiswirth, F.W. Schneider, Physica D **63**, 117 (1993).
19. F. Takens, *Dynamical systems and turbulence*, Springer Lecture Notes in Mathematics **868** (New-york, Springer Verlag, 1981), p. 366.
20. E. Gravier, X. Caron, G. Bonhomme, Th. Pierre, Phys. Plasmas (to be published, 1999).
21. W. Just, T. Bernard, M. Ostheimer, E. Reibold, H. Benner, Phys. Rev. Lett. **78**, 203 (1997).
22. G. Hu, Z. Qu, Phys. Rev. Lett. **72**, 68 (1994).
23. D. Auerbach, Phys. Rev. Lett. **72**, 1184 (1994).
24. G.A. Johnson, M. Locher, E.R. Hunt, Phys. Rev. E **51**, R1625 (1995).
25. J. Jiang, A. Antillon, P. Parmananda, J. Escalona, Phys. Rev. E **56**, 2568 (1997).
26. N. Parekh, V. Ravi Kumar, B.D. Kulkami, Chaos **8**, 300 (1998).
27. A. Amengual, E. Hernandez-Garcia, R. Montagne, M. San Miguel, Phys. Rev. Lett. **78**, 4379 (1997).
28. L. Kocarev, U. Parlitz, Phys. Rev. Lett. **77**, 2206 (1996).
29. J. Yang, G. Hu, J. Xiao, Phys. Rev. Lett. **80**, 496 (1998).
30. N.F. Rulkov, M.M. Sushchik, L.S. Tsimring, H.D.I. Abarbanel, Phys. Rev. E **51**, 980 (1995).
31. G. Hu, J. Xiao, J. Yang, F. Xie, Z. Qu, Phys. Rev. E **56**, 2738 1997.
32. K. Murali, M. Lakshmanan, Phys. Rev. E **49**, 4882 (1994).
33. T. Kapitaniak, Phys. Rev. E **50**, 1642 (1994).
34. H. Chaté, P. Manneville, Physica D **32**, 409 (1988).
35. P. Bergé, Y. Pomeau, C. Vidal, *L'espace chaotique* (Hermann, 1988).